Photoelectrochemistry

Deutsche Ausgabe: DOI: 10.1002/ange.201510869
Internationale Ausgabe: DOI: 10.1002/anie.201510869

Acid Treatment Enables Suppression of Electron–Hole Recombination in Hematite for Photoelectrochemical Water Splitting

Yi Yang, Mark Forster, Yichuan Ling, Gongming Wang, Teng Zhai, Yexiang Tong, Alexander J. Cowan, and Yat Li**

Abstract: *We report a strategy for efficient suppression of electron–hole recombination in hematite photoanodes. Acid-treated hematite showed a substantially enhanced photocurrent density compared to untreated samples. Electrochemical impedance spectroscopy studies revealed that the enhanced photocurrent is partly due to improved efficiency of charge separation. Transient absorption spectroscopic studies coupled to electrochemical measurements indicate that, in addition to improved bulk electrochemical properties, acid-treated hematite has significantly decreased surface electron–hole recombination losses owing to a greater yield of the trapped photoelectrons being extracted to the external circuit.*

Hematite has been extensively studied as photoanodes for water splitting.[1–5] Nevertheless, poor hole transfer efficiency and late turn-on characteristics limits their photoelectrochemical (PEC) performance.[6,7] To address these limitations, a number of hematite nanostructures have been developed to minimize hole transfer distance.[1,8,9] Surface passivation has been found to be another effective method to enhance hole transfer efficiency by reducing the number of surface trap states.[6,7,10] Likewise, hole transfer efficiency can be improved by decorating the hematite surface with oxygen evolution reaction catalysts, which can enhance activity either by reducing the over-potential for water oxidation[11–13] or through the suppression of slow recombination owing to interfacial electronic effects.[14–16] Previous studies also suggested that the turn-on characteristics of hematite photoanodes may be closely related to their surface nature.[17,18] Jang et al. reported a re-growth strategy to reduce surface disorders of hematite and achieved a significantly shifted onset voltage.[17] Yet, the performance of hematite photoanodes can also be limited by the efficiency of initial charge separation and electron transfer, which has been rarely studied. Herein, we demonstrate that a simple acid treatment method can substantially enhance the efficiency of electrons moving out of traps in hematite nanowire photoanodes, and therefore reduce the electron–hole recombination loss and improve PEC performance.

Hematite nanowires intentionally doped with Sn were synthesized on a FTO glass substrate according to reported methods (Supporting Information).[9] Nanowires are vertically aligned on the FTO substrate, with average diameter of 100 nm and length of ≈1 μm (Supporting Information, Figure S1 a). The hematite nanowire film was immersed in pure acetic acid solution for 5 min, followed by annealing in air at 450 °C for 30 min. The nanowire morphology and crystal phase remained unchanged upon acid treatment and annealing (Figures S1b and S2). The acid-treated hematite also had a smooth surface similar to the untreated sample, with no sign of surface etching or shell coating (Figure S3), as well as comparable surface area (Figure S4). X-ray photoelectron spectroscopy (XPS) was used to investigate the possible influence of acid treatment on the chemical nature of the hematite surface (Figure S5). Both untreated and acid-treated samples exhibited a Fe 2p1/2 peak and a Fe 2p3/2 peak centered at binding energies of 724.5 eV and 711.4 eV, which are typical values reported for Fe^{3+} in Fe_2O_3.[19] Notably, acid-treated hematite had a slightly higher Fe^{2+} signal (a satellite peak located at 716 eV)[20] than the untreated sample, suggesting that Fe^{2+} sites were created during acid treatment. Acid-treated hematite also exhibited an additional shoulder peak at 531.9 eV that can be attributed to Fe−OH, which has been reported to be located at a binding energy 1.5–2.0 eV higher than the O 1s peak of Fe_2O_3.[21] The XPS data confirm the increased amount of hydroxy groups on the hematite surface following acid treatment, resulting in the formation of more Fe^{2+} sites to balance the charge.

Acid-treated hematite showed considerably enhanced photocurrent density compared to that of the untreated sample (Figure 1 a). To understand the effect of thermal annealing on the performance of hematite we also collected I-V curves from the hematite sample without acid treatment but thermally annealed under the same conditions. The untreated but thermally annealed sample exhibited comparable photocurrent densities as the untreated sample (Figure S6), indicating that the combination of acid treatment and the subsequent thermal annealing process is essential for the enhanced performance of the acid-treated sample. As expected, the acid-treated hematite also exhibits significantly enhanced incident photon-to-current conversion efficiency (IPCE) values compared to the untreated sample over the

[*] Y. Yang, Dr. Y. Ling, Dr. G. Wang, Dr. T. Zhai, Prof. Y. Li
Department of Chemistry and Biochemistry
University of California, Santa Cruz
Santa Cruz, CA 95064 (USA)
E-mail: yatli@ucsc.edu
M. Forster, Prof. A. J. Cowan
Department of Chemistry and Stephenson
The University of Liverpool
Liverpool L69 7ZD (UK)
E-mail: A.J.Cowan@liverpool.ac.uk
Dr. T. Zhai, Prof. Y. Tong
School of Chemistry and Chemistry Engineering
Sun Yat-Sen University
Guangzhou 510275 (P.R. China)

Supporting information for this article can be found under http://dx.doi.org/10.1002/anie.201510869.

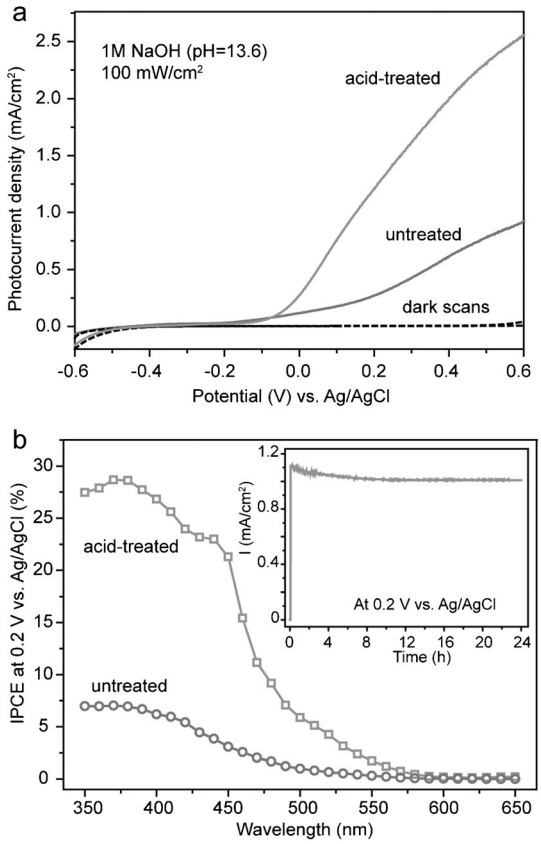

Figure 1. a) I–V curves collected for untreated and acid-treated hematite photoaonodes at 20 $mV s^{-1}$ in a 1 M NaOH electrolyte solution under illumination by simulated solar light of 100 $mW cm^{-2}$ and in the dark. b) IPCE spectra of untreated and acid-treated hematite samples. Inset: I–t curve of acid-treated hematite.

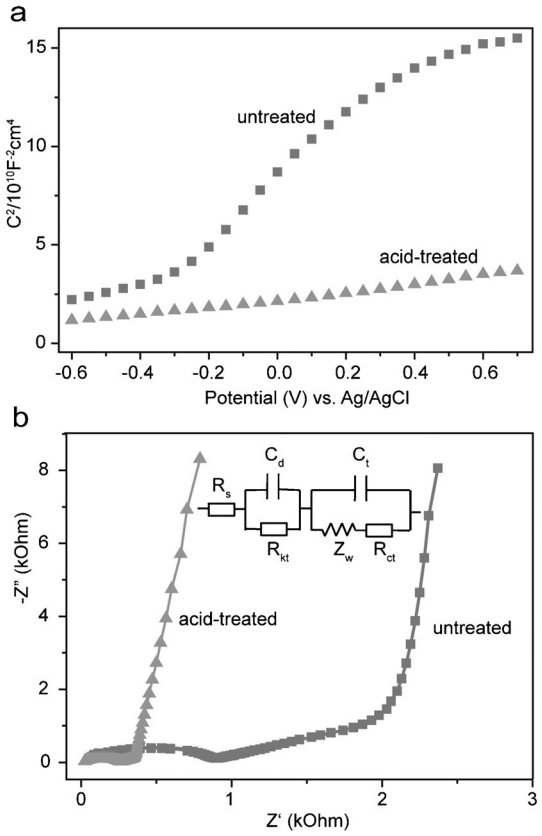

Figure 2. a) Mott–Schottky plots of untreated and acid-treated hematite electrodes collected at 10 kHz in the dark. b) EIS spectra of untreated and acid-treated hematite electrodes. Inset: equivalent circuit used to fit the spectra (Supporting Information).

entire spectrum we studied. IPCE values of both samples gradually dropped to zero at wavelengths beyond 600 nm, in accordance with the band gap of hematite. There was no obvious change in the light absorption capability of hematite upon acid treatment (Figure S7). Taken together, these results indicate that the enhanced photocurrent density of acid-treated hematite is due to improved efficiency of charge collection following light harvesting. Furthermore, the acid-treated hematite shows excellent photostability (Figure 1b, inset), showing that the enhanced photocurrent is not at the expense of photostability. In addition to acetic acid, we also tested other inorganic acids, including HCl, HNO_3, and H_3PO_4, for treating hematite nanowire films. The hematite films treated with different acids all showed pronounced enhancements in their photocurrents (Figure S8), indicating that acid treatment is a general strategy for enhancing the performance of hematite photoanodes.

We investigated the influence of acid treatment on the electronic properties of hematite and its possible relation to the enhanced charge collection efficiency and photoactivity. Figure 2a shows the Mott–Schottky plots generated based on the capacitances derived from the electrochemical impedance values obtained at each potential. The donor density of acid-treated hematite was calculated to be 1.11×10^{20} cm^{-3}, which is an order of magnitude higher than that of the untreated sample (1.06×10^{19} cm^{-3}). Meanwhile the donor density of thermally annealed hematite without acid treatment (1.23×10^{19} cm^{-3}) is very similar to the untreated sample (Figure S9). The increased donor density is expected to improve the electrical conductivity of hematite, and therefore reduce the electrode internal resistance and the voltage drop at the interface of hematite and FTO substrate. Furthermore, electrochemical impedance spectroscopy (EIS) measurements were used to investigate the influence of acid treatment on the charge transfer at the hematite/electrolyte interface. The Nyquist plots of hematite electrodes consist of a semicircle in the high-frequency domain and a steep line in the low-frequency domain (Figure 2b). The inset of Figure 2b shows the equivalent circuit used to fit the EIS data. Significantly, the charge transfer resistance (R_{ct}) of hematite was considerably reduced from 113.6 Ω to 5.1 Ω after acid treatment (Table S1). The reduced R_{ct} can be attributed to the improved electrical conductivity of acid-treated hematite.

It is anticipated that the acid treatment primarily modifies the surface properties of the hematite electrode. However, in light of the measured increased donor density, it is also important to assess if the improved activity can, at least in part, be related to a difference in the yield of initial charge separation, which is defined as the yield of photogenerated holes reaching the surface. Sivula et al. previously described a simple methodology for distinguishing between bulk and

surface electron–hole recombination losses,[22] where the photoelectrochemical response in the presence of H_2O_2, an efficient hole scavenger, is compared to that achieved during water oxidation. Similar experiments performed here indicate that we achieved a slight decrease in bulk-electron hole recombination, with the yield of photoholes reaching the surface increasing from 33% to nearly 50% for acid-treated hematite at 0.2 V versus Ag/AgCl (Figure S10). Whilst significant, this change in charge separation yield alone is not sufficient to explain the very large change in IPCE measured during water splitting, which at 0.2 V versus Ag/AgCl, 350 nm, increases approximately four-fold (7% to 27%; Figure 1b). This indicates that a change in the surface kinetics is likely to be a more significant factor controlling the enhanced activity.

Transient absorption (TA) spectroscopy and transient photocurrent (TPC) measurements allow the direct measurement of the yield and dynamics of photogenerated charges within a photoelectrode. Previous TA spectroscopic studies of hematite photoelectrodes have examined numerous aspects of the photophysics and chemistry of extrinsically and intrinsically doped hematite, including the role of co-catalysts on hole kinetics, the effect of bias on charge trapping and recombination, and the effect of surface passivation on trap states, from the fs–ms timescale.[9,23,24] In line with these past studies, the TA spectra (500–825 nm) of the untreated and acid-treated samples, at a potential (0.2 V versus Ag/AgCl) where water oxidation is expected to occur, show two distinct features that are well documented for hematite:[24–26] a broad positive transient absorption at wavelengths greater than $\approx$600 nm, and a sharp bleach at $\approx$575 nm, which are assigned to photoholes and trapped photoelectrons, respectively (Figure 3a,b). The similar magnitude of the maximum transient signal at 575 nm (-1×10^{-4} O.D.; Figure 4) indicates that, following the initial charge separation, a similar yield of photoelectrons are trapped at inter-band states in both films. However, we find that the rate of recovery of the 575 nm bleach, that is, the rate of loss of trapped electrons, is markedly accelerated following the acid treatment, and can be fitted to a single-exponential decay function with a time constant of 7 ± 1 ms for the acid-treated sample and 40 ± 4 ms for the untreated sample. Trap-mediated electron–hole recombination at or close to the hematite surface has been shown to be a significant loss pathway in several studies,[23,27–29] and here we explored the fate of the de-trapped electrons measured by TA through comparison to the recorded transient photocurrent (Figure 4; Figure S11). In both samples, the rate of decay of the 575 nm TA signal is similar to the rate of charge extraction as measured by TPC (Figure 4b), indicating that a portion of the de-trapped electrons are able to reach the external circuit. However, despite the similar initial concentrations of trapped electrons, we noted a far lower charge-extraction yield in the untreated sample (Figure 4b). This indicates that, in parallel to electron transport to the external circuit, a second process is occurring which dominates in the untreated sample. We assign the parallel process to recombination, which on this timescale is anticipated to be with surface-trapped holes. We propose a simple parallel kinetics model where the trapped electrons

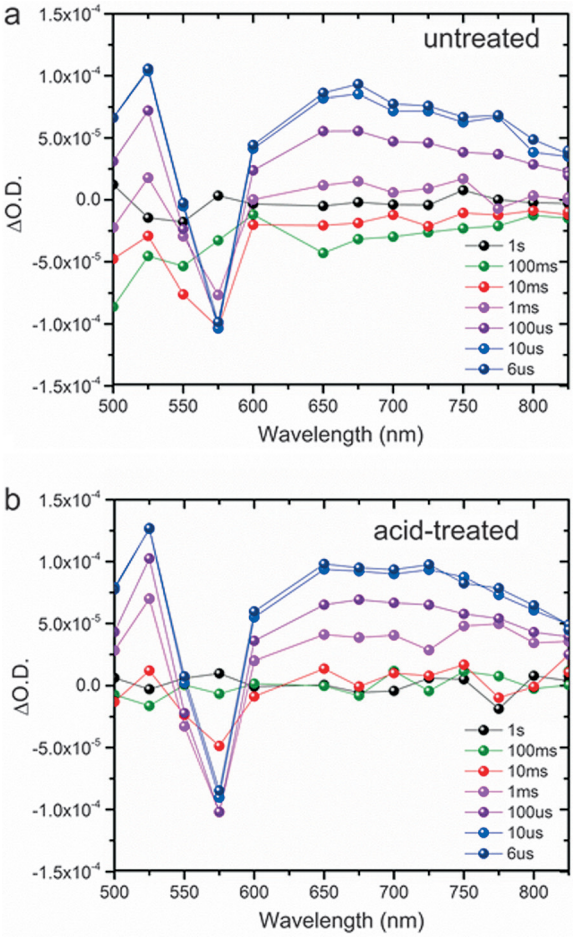

Figure 3. Full spectra TA under working photoelectrochemical conditions (355 nm excitation) at an applied voltage of 0.2 V vs. Ag/AgCl for a) untreated and b) acid-treated hematite.

can either be extracted to the external circuit to give rise to a photocurrent, or be lost through recombination with trapped holes, with the two processes having rate constants k_{ext} and k_{rec}, respectively (Figure S12). In our kinetics model, the overall rate of loss of the trapped electrons is given by the sum of the parallel rate constants, and the yield of each pathway is determined by the relative rate constants of the processes. A full kinetic analysis is presented in the Figure S13.[30] The greater relative rate constant for the detrapping and charge-extraction pathway following acid treatment gives rise to a higher charge extraction yield. TA spectroscopic (Figure S14) and TPC measurements of a hematite film that has undergone thermal annealing without acid treatment showed only a slight change in the rate (Figure S15) and yield of charge-extracted (Figure 4) when compared to the untreated sample, again confirming that both the acid treatment and the subsequent thermal annealing process are required for improved performance. This indicates that the combined acid and thermal treatments modify either the nature or position of the available trap sites. In this study, we are unable to definitively ascertain the spatial positioning of the trap sites within the film. However, the acid treatment would be expected to primarily affect surface states. Jang

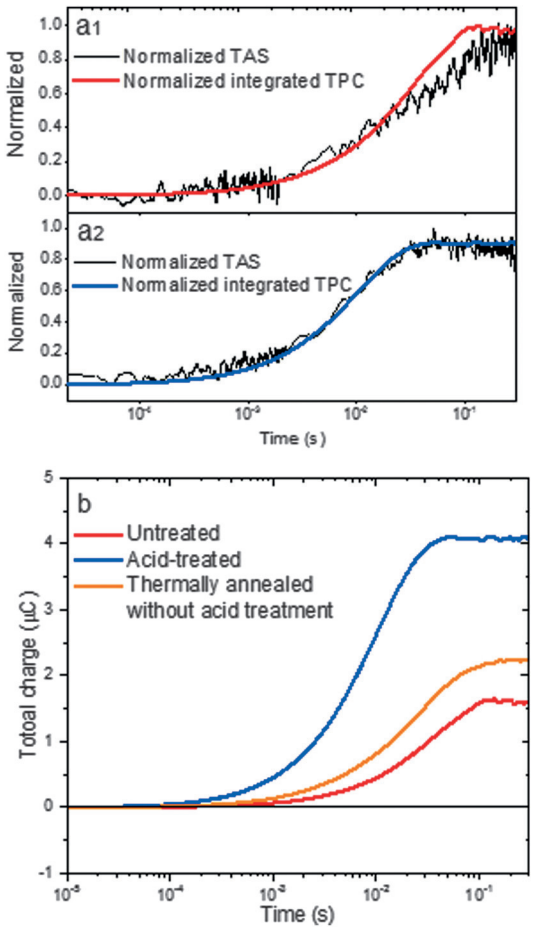

Figure 4. Overlay of 575 nm TA signal assigned to photoelectron trapping with the total charge passed derived from TPC following 355 nm excitation of a1) untreated and a2) acid-treated hematite at 0.2 V vs. Ag/AgCl. b) The charge extracted with time before normalization for the photoelectrodes studied.

et al. also recently proposed a re-growth approach to hematite that modifies surface defects.[17] In addition, Cao et al. reported that the surface-trapped electrons are involved in the back reaction for oxygen reduction.[31] The enhanced rate of detrapping photo-electrons can suppress the back reaction.

In summary, we have demonstrated that acid treatment can substantially increase the performance of hematite photoanodes for PEC water splitting. EIS studies have shown that enhanced photocurrent is partly due to improved efficiency of charge separation. Moreover, TA and TPC spectroscopic studies provide evidence that the improved efficiency can also be related to a minimization of surface electron–hole recombination brought about by an increased detrapping rate, in line with the improved conductivity and potential passivation of surface electron traps. We believe that these studies open up new opportunities for the design and fabrication of high performance hematite electrodes for PEC reactions.

Acknowledgements

AJC gratefully acknowledges a fellowship from the EPSRC (EP/K006851/1). We acknowledge Dr. Tom Yuzvinsky for SEM image acquisition and the W. M. Keck Center for Nanoscale Optofluidics for use of the FEI Quanta 3D Dual-beam microscope. We thank Jesse Hauser for XRD measurement and the support of UCSC XRD (Rigaku Americas Mini flex Plus powder diffractometer) facility supported by the U.S. NSF MRI grant (MRI-1126845).

Keywords: acid treatment · hematite · metal oxides · photoelectrochemical water splitting · transient absorption spectroscopy

How to cite: *Angew. Chem. Int. Ed.* **2016**, *55*, 3403–3407
Angew. Chem. **2016**, *128*, 3464–3468

[1] A. Kay, I. Cesar, M. Gratzel, *J. Am. Chem. Soc.* **2006**, *128*, 15714–15721.
[2] C. Kronawitter, I. Zegkinoglou, S. Shen, P. Liao, I. Cho, O. Zandi, Y. Liu, K. Lashgari, G. Westin, J. Guo, F. Himpsel, E. Carter, X. Zheng, T. Hamann, B. Koel, S. Mao, L. Vayssieres, *Energy Environ. Sci.* **2014**, *7*, 3100–3121.
[3] W. Li, D. He, Y. He, X. Yao, R. Grimm, G. Brudvig, D. Wang, *Angew. Chem. Int. Ed.* **2015**, *54*, 11428–11432; *Angew. Chem.* **2015**, *127*, 11590–11594.
[4] C. Du, M. Mayer, H. Hoyt, J. Xie, G. McMahon, G. Bischoping, D. Wang, *Angew. Chem. Int. Ed.* **2013**, *52*, 12692–12695; *Angew. Chem.* **2013**, *125*, 12924–12927.
[5] M. Zhou, H. Wu, J. Bao, L. Liang, X. Lou, Y. Xie, *Angew. Chem. Int. Ed.* **2013**, *52*, 8579–8583; *Angew. Chem.* **2013**, *125*, 8741–8745.
[6] T. Hisatomi, F. Le Formal, M. Cornuz, J. Brillet, N. Tetreault, K. Sivula, M. Gratzel, *Energy Environ. Sci.* **2011**, *4*, 2512–2515.
[7] F. Le Formal, N. Tetreault, M. Cornuz, T. Moehl, M. Gratzel, K. Sivula, *Chem. Sci.* **2011**, *2*, 737–743.
[8] J. Brillet, M. Gratzel, K. Sivula, *Nano Lett.* **2010**, *10*, 4155–4160.
[9] Y. Ling, G. Wang, D. Wheeler, J. Zhang, Y. Li, *Nano Lett.* **2011**, *11*, 2119–2125.
[10] R. Liu, Z. Zheng, J. Spurgeon, X. Yang, *Energy Environ. Sci.* **2014**, *7*, 2504–2517.
[11] P. Liao, J. Keith, E. Carter, *J. Am. Chem. Soc.* **2012**, *134*, 13296–13309.
[12] K. Sun, N. Park, Z. Sun, J. Zhou, J. Wang, X. Pang, S. Shen, S. Noh, Y. Jing, S. Jin, P. Yu, D. Wang, *Energy Environ. Sci.* **2012**, *5*, 7872–7877.
[13] G. Wang, Y. Ling, X. Lu, T. Zhai, F. Qian, Y. Tong, Y. Li, *Nanoscale* **2013**, *5*, 4129–4133.
[14] M. Barroso, A. Cowan, S. Pendlebury, M. Gratzel, D. Klug, J. Durrant, *J. Am. Chem. Soc.* **2011**, *133*, 14868–14871.
[15] Y. Ma, A. Kafizas, S. Pendleburya, J. Durrant, *J. Mater. Chem. A*, **2015**, *3*, 20649-20657.
[16] C. Cummings, F. Marken, L. Peter, A. Tahir, K. Wijayantha, *Chem. Commun.* **2012**, *48*, 2027–2029.
[17] J. Jang, C. Du, Y. Ye, Y. Lin, X. Yao, J. Thorne, E. Liu, G. McMahon, J. Zhu, A. Javey, J. Guo, D. Wang, *Nat. Commun.* **2015**, *6*, 7447.
[18] I. Cho, H. Han, M. Logar, J. Park, X. Zheng, *Adv. Energy Mater.* **2015**, DOI: 10.1002/aenm.201501840.
[19] G. Wang, H. Wang, Y. Ling, Y. Tang, X. Yang, R. Fitzmorris, C. Wang, J. Zhang, Y. Li, *Nano Lett.* **2011**, *11*, 3026–3033.
[20] L. Xi, S. Chiam, W. Mak, P. Tran, J. Barber, S. Loo, L. Wong, *Chem. Sci.* **2013**, *4*, 164–169.

[21] T. Jeon, W. Choi, H. Park, *J. Phys. Chem. C* **2011**, *115*, 7134 – 7142.
[22] H. Dotan, K. Sivula, M. Gratzel, A. Rothschild, S. Warren, *Energy Environ. Sci.* **2011**, *4*, 958 – 964.
[23] M. Forster, Y. Ling, Y. Yang, D. Klug, Y. Li, A. J. Cowan, *Chem. Sci.*, **2015**, *6*, 4009-4016.
[24] M. Barroso, S. Pendlebury, A. J. Cowan, J. Durrant, *Chem. Sci.* **2013**, *4*, 2724 – 2734.
[25] A. J. Cowan, C. Barnett, S. Pendlebury, M. Barroso, K. Sivula, M. Gratzel, J. Durrant, D. Klug, *J. Am. Chem. Soc.* **2011**, *133*, 10134 – 10140.
[26] S. Pendlebury, A. J. Cowan, M. Barroso, K. Sivula, J. Ye, M. Gratzel, D. Klug, J. Tang, J. Durrant, *Energy Environ. Sci.* **2012**, *5*, 6304 – 6312.
[27] K. Sivula, *J. Phys. Chem. Lett.* **2013**, *4*, 1624 – 1633.
[28] L. Steier, I. H. Cardona, S. Gimenez, F. F. Santiago, J. Bisquert, S. D. Tilley, M. Gratzel, *Adv. Funct. Mater.* **2014**, *24*, 7681 – 7688.
[29] O. Zandi, T. W. Hamann, *J. Phys. Chem. Lett.* **2014**, *5*, 1522 – 1526.
[30] P. Michael J. Pilling, *Reaction Kinetics*, 2nd ed., Oxford University Press, Oxford, **1996**.
[31] D. Cao, W. Luo, J. Feng, X. Zhao, Z. Li, Z. Zou, *Energy Environ. Sci.* **2014**, *7*, 752 – 759.

Received: November 30, 2015
Revised: December 22, 2015
Published online: February 5, 2016

